JOURNAL OF GEOPHYSICAL RESEARCH, VOL. 113, C04026, doi:10.1029/2006JC004063, 2008

Subpolar Mode Water in the northeastern Atlantic: 2. Origin and transformation

Elena Brambilla,[1] Lynne D. Talley,[1] and Paul E. Robbins[1]

Received 14 December 2006; revised 8 August 2007; accepted 12 December 2007; published 23 April 2008.

[1] The processes that lead to the transformation and origin of the eastern North Atlantic Subpolar Mode Waters (SPMW) are investigated from observational data using an extended Walin framework. Air-sea flux data from the National Oceanography Center, Southampton (NOCS), and hydrographic data from the A24 cruise collected during the World Ocean Circulation Experiment (WOCE) are used to estimate the contribution of diapycnal and isopycnal fluxes to the density classes that include SPMW. Surface diapycnal volume flux is the dominant source of waters in the SPMW density. In the North Atlantic subpolar gyre the diapycnal volume flux occurs along the main branches of the North Atlantic Current (NAC) and it has an average transport of 14 ± 6.5 *Sv*, with a maximum of 21.5 Sv across the $27.35\sigma_\theta$ isopycnal. The regional distribution of the diapycnal flux on isopycnal surfaces is computed to identify the areas with the largest diapycnal flux. These regions coincide with the location of SPMW based on potential vorticity. The surface diapycnal flux is associated with obduction and subduction through the permanent pycnocline. Therefore, the water involved in the transformation of SPMWs is continuously exchanged with the ocean interior. In addition, we suggest that subduction is not associated with smooth advection from the mixed layer to the ocean interior, but is water mass loss entrainment into the deep overflows of the subpolar gyre. The isopycnal component of the SPMW throughput is estimated from the geostrophic transport across the A24 section from Greenland to Scotland and is 10% to 40% of the diapycnal flux.

Citation: Brambilla, E., L. D. Talley, and P. E. Robbins (2008), Subpolar Mode Water in the northeastern Atlantic: 2. Origin and transformation, *J. Geophys. Res.*, *113*, C04026, doi:10.1029/2006JC004063.

1. Introduction

[2] Mode waters are water masses characterized by thick layers of nearly vertically uniform properties (potential temperature, salinity, potential density) that extend over a relatively large horizontal area [*Hanawa and Talley*, 2001]. *Masuzawa* [1969] first introduced the term "Subtropical Mode Water" to refer to a thick layer of water with nearly uniform temperature (16°–18°C) in the northwestern North Pacific subtropical gyre. *McCartney and Talley* [1982] introduced the term "Subpolar Mode Water" to describe the mode water masses confined in the North Atlantic subpolar gyre.

[3] The northward transport of warm and salty water from low latitudes to the sites of dense water formation occurs in the surface layer, which is dominated in the subpolar gyre by the SPMW water mass [e.g., *McCartney and Talley*, 1982, 1984; *Schmitz and McCartney*, 1993; *McCartney and Mauritzen*, 2001]. In the first part of our SPMW study [*Brambilla and Talley*, 2008], we detailed the hydrographic properties, the vertical and horizontal sites occupied by SPMWs, and the link between SPMW and the branches of the North Atlantic Current (NAC) in the subpolar gyre. Here, we investigate the major sources, processes and locations for SPMW transformation, subduction (entrainment), and obduction.

[4] *McCartney and Talley* [1982] hypothesized that SPMWs, homogenized during winter deep convection events, were advected by a cyclonic flow in the subpolar gyre, increasing their density along the path owing to heat loss. Therefore they hypothesized that each SPMW is the source of SPMW of higher density. The hypothesis of smooth, cyclonic progression completely around the subpolar gyre has been partially revised [e.g., *Talley*, 1999; *Read*, 2001; *Perez-Brunius et al.*, 2004].

[5] In the first part [*Brambilla and Talley*, 2008], we showed that SPMWs dominate the surface layer along the warm side of each of the several branches of the North Atlantic Current (NAC). We showed that the averaged paths of the Rockall Trough and Iceland Basin branches of the NAC are characterized by their own sequence of SPMWs of increasing density following the flow downstream (*Brambilla and Talley*'s [2008] Figure 1, reproduced here as Figure 1). Since the eastern subpolar gyre flow is predominantly northeastward, carrying water from the subtropical North Atlantic to the Norwegian Current, *McCartney and Talley*'s [1982] concept of overall cyclonic circulation of SPMWs around the subpolar gyre is not accurate. Hence, we concluded that the most likely origin of an SPMW of a certain density is the lighter SPMW

[1]Scripps Institution of Oceanography, University of California, San Diego, La Jolla, California, USA.

0148-0227/08/2006JC004063$09.00

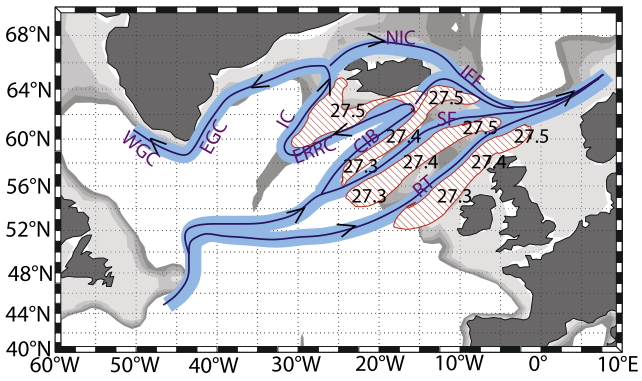

Figure 1. Schematic of the mean currents (light blue) present in the subpolar gyre and the SPMW (red) associated with them [*Brambilla and Talley*, 2008]. On the SPMW patch is written the density sequence. The darker lines represent the current fronts. SPMWs are found on the warm side of the current. The current names are as follows: RT, Rockall Trough Branch of the NAC; SF, Subarctic Front; CIB, Central Iceland Basin Branch of the NAC; ERRC, East Reykjanes Ridge Current; IC, Irminger Current; NIC, North Iceland Current; IFF, Iceland Faroe Front; EGC, East Greenland Current; WGC, West Greenland Current.

upstream only if the two water masses are associated with the same current branch. Here, we focus on the contribution of isopycnal and diapycnal fluxes to the SPMW throughput. The isopycnal flux is simply measured in terms of geostrophic transport. The diapycnal flux is examined using the *Walin* [1982] framework for water mass transformation driven by air-sea interaction. SPMWs are the dominant water masses in the upper layer from the ocean surface to the permanent pycnocline [*McCartney and Talley*, 1982; *Brambilla and Talley*, 2008]. Within this surface layer, the water masses (e.g., SPMW) are transformed by air-sea interaction. Therefore, the surface diapycnal volume flux can be used as a measurement of the transformation rate in the SPMW density range.

[6] Estimates of water mass transformation rates in the North Atlantic have been the subject of many studies [e.g., *Tziperman*, 1986; *Garrett et al.*, 1995; *Garrett and Tandon*, 1997; *Nurser et al.*, 1999]. Hydrographic measurements and air-sea flux data have been used to compute both the annual mean, zonally integrated meridional stream function [*Marsh*, 2000] and the basin-integrated water mass formation [*Speer and Tziperman*, 1992; *Speer et al.*, 1995; *Speer*, 1997]. Model output data [*Marshall et al.*, 1999; *Gulev et al.*, 2003; *Valdivieso Da Costa et al.*, 2005] or hydrographic data combined in an inverse model method [*Lumpkin and Speer*, 2003] have been used for the same purpose.

[7] In the mentioned papers, the water mass transformation rate in the North Atlantic subpolar gyre is subsumed in the global basin-scale analysis [e.g., *Speer*, 1997; *Marsh*, 2000], or is only partially represented because of data limitation at northern latitudes ($\phi < 65°$N) [e.g., *Speer and Tziperman*, 1992; *Valdivieso Da Costa et al.*, 2005]. Here, we focus on the subpolar North Atlantic and the southern Nordic Seas to 75°N and compute the transformation rates for water masses characterized by potential density greater than $27\sigma_\theta$. Moreover, in addition to the basin-integrated annual mean transformation, we examine the regional distribution of the annual mean transformation for each potential density. This allows us to identify the specific areas where the transformations are more intense. Then, combining the annual mean regional distribution of the water mass transformation rates with the surface circulation based on surface drifters [*Brambilla and Talley*, 2008], we identify the currents that provide water to the intense transformation regions.

[8] These estimates of water mass transformation represent the diapycnal contribution to the SPMW throughput. However isopycnal flux might also be relevant. Therefore we roughly estimate the contribution of the isopycnal flux by examining the baroclinic component of the geostrophic flow across a hydrographic transect that crosses the eastern subpolar gyre (Greenland-Scotland).

[9] Section 2 describes the data and the methods used. In section 3, we discuss the surface water mass transformation due to air-sea fluxes. Section 4 describes the formation and obduction areas for specific isopycnal surfaces. In section 5, we examine the contribution of the isopycnal flux to SPMW transport. Section 6 summarizes the results.

2. Data and Methods

2.1. Data

[10] Air-sea flux and hydrographic data, along with stream functions calculated by *Brambilla and Talley* [2008], are used to investigate the water masses and the currents involved in the origin of SPMW in the northeastern Atlantic.

[11] The air-sea flux data are from the "adjusted" air-sea flux climatology from the National Oceanography Center, Southampton (NOCS). This data set represents an improved version of the original heat flux climatology from NOCS [*Grist and Josey*, 2003]. In the adjusted data set, the data have been constrained to hydrographic measurements using a mathematical inverse method to reduce the imbalance of the global mean net ocean heat flux to -5 W/m^2 [*Grist and Josey*, 2003]. The data used in this research are monthly mean heat flux and monthly mean evaporation minus precipitation in the region 10°N–75°N, 100°W–20°E. Both data types are provided on a regular $1° \times 1°$ grid.

[12] Monthly mean climatological hydrographic data are used, objectively mapped on a regular $1° \times 1°$ grid, from the World Ocean Atlas 2001 (WOA01) [*Conkright et al.*, 2002]. Synoptic hydrographic data from the A24 cruise (May–July 1997) during the World Ocean Circulation Experiment (WOCE) are used. The WOA01 data are used in the computation of the water mass transformation rates (section 2.2) while the cruise data are used to compute geostrophic transport across the hydrographic section.

2.2. Computation of the Water Mass Transformation and Formation

2.2.1. Background

[13] Water mass formation in a certain density class can be computed using either a dynamic or a thermodynamic method [*Marshall et al.*, 1999]. The former measures the rate at which the water mass crosses from the surface mixed layer into the permanent pycnocline. It depends on the time

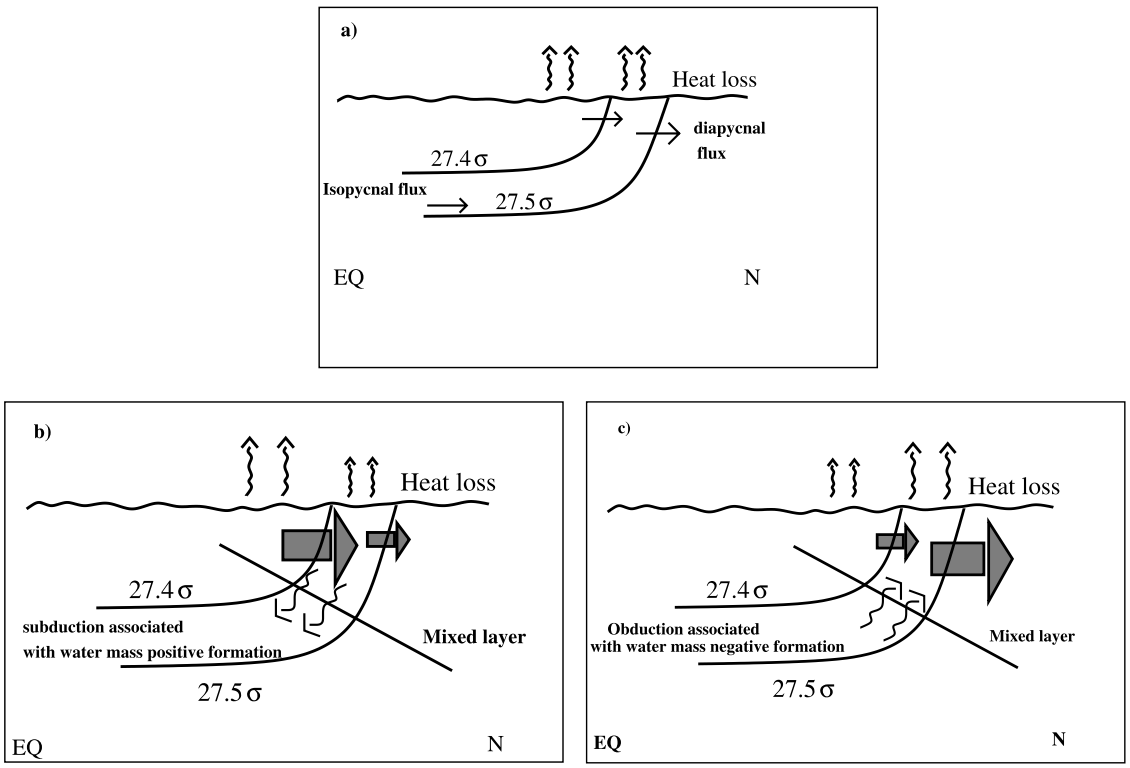

Figure 2. Schematics to describe the processes of instantaneous transformation and formation (positive and negative). (a) Transformation of surface water masses from a given density to the next highest density. This is equivalent to diapycnal flux. (b) Positive water mass formation associated with subduction from the surface mixed layer into the ocean interior driven by the convergence of surface water mass transformation. (c) Negative water mass formation associated with obduction from the ocean interior to the surface mixed layer driven by the divergence of surface water mass transformation.

variability of the mixed layer depth and the horizontal transport through the mixed layer [*Marshall et al.*, 1993]. In contrast, the thermodynamic method, used here, is based on the relation derived by *Walin* [1982] between water mass formation and heat fluxes. Combining heat and volume budgets, he showed that the diapycnal volume flux across an outcropping isopycnal is equivalent to the transformation of surface water from one particular density class to another surface density class. The convergence (divergence) of this transformation yields the water mass formation (obduction) rate.

[14] As pointed out by *Garrett et al.* [1995], and later by *Marshall et al.* [1999], the equivalence between the diapycnal volume flux and the air-sea transformation is valid only with specific a priori assumptions. They showed that air-sea fluxes are not the only forcing involved in the water mass transformation; indeed vertical mixing processes across the base of the mixed layer act to reduce the density changes related to air-sea interaction. Because light water tends to spread over dense water, and therefore requires a poleward diapycnal volume flux [*Walin*, 1982], vertical mixing is particularly important at subtropical latitudes to counteract air-sea flux that transforms water toward lighter density [*Marshall et al.*, 1999]. In the subpolar gyre, in contrast, since most of the mixing occurs by lateral flux through the almost vertical isopycnals of the mixed layer, vertical mixing is likely small and the relation between diapycnal volume flux and the air-sea flux can still be applied [*Nurser et al.*, 1999; *Marsh*, 2000; *Valdivieso Da Costa et al.*, 2005; *Tandon and Zhao*, 2004].

[15] Numerous studies of water mass transformation describe the relation between the diapycnal volume flux and the surface water mass transformation [e.g., *Tziperman*, 1986; *Garrett et al.*, 1995; *Marshall et al.*, 1999; *Large and Prince*, 2001]. The remainder of this section and Figure 2 are a brief summary to provide essential background.

[16] As described by *Tziperman* [1986], at fixed time t, surface buoyancy loss over the outcrop area of isopycnal $\sigma_\theta^{[1]}$ (where σ_θ is the mean potential density of the outcrop, and the superscript is an index of the outcrop density of the isopycnal) increases the density to a new value $\sigma_\theta^{[2]}$ ($\sigma_\theta^{[1]} < \sigma_\theta^{[2]}$). If there is also buoyancy loss within the $\sigma_\theta^{[2]}$ outcrop area, the surface water mass continues increasing its density, for example, to a new density $\sigma_\theta^{[3]}$. If the volume leaving the $\sigma_\theta^{[1]}$ outcrop area is larger than the volume leaving the $\sigma_\theta^{[2]}$ area, there is a convergence that leads to subduction, or positive "formation", of the water mass with density $\sigma_\theta^{[2]}$. Following *Speer and Tziperman* [1992] the word "transformation" refers to the diapycnal flux at the ocean surface from one density to the next density class and so on (Figure 2a). Given the equivalence between diapycnal volume flux and water mass transformation, the two expressions are used interchangeably.

[17] When there is convergence or divergence of the surface water mass transformation, then there is a loss or gain of water through the base of the surface layer; these are

referred to as positive or negative "formation." Positive and negative formation are often identified with the processes of subduction and obduction (Figures 2b and 2c). (However, we see below for the denser, northeastern SPMWs that there can be formation without classical subduction, which is normally associated with wind-forced downwelling and lateral induction [*Marshall et al.*, 1993]. Here "formation" appears to be due to turbulent entrainment of surface layer waters by underlying overflow waters.) Mathematically, the proportionality between air-sea flux and water mass transformation, integrated in time and space, can be written

$$\overline{F(\sigma_\theta)} = \frac{1}{\Delta T \Delta \sigma} \int_{year} dt \int \int_{area} dA \delta\left(\sigma'_\theta(x,y,t) - \sigma_\theta\right) f(x,y,t). \tag{1}$$

$\overline{F(\sigma_\theta)}$ is the annual mean water mass transformation function (diapycnal volume flux m^3/s); the overbar is the annual average over the density outcrop, $\Delta T = 1$ year, $\Delta\sigma = 1$ kg/m^3. (Equation (1) follows *Speer and Tziperman*'s [1992] computation, with some differences in the notation. In the work by *Speer and Tziperman* [1992] the function F indicates the total density flux for 1 year as a function of sea surface density, equivalent to the total diapycnal mass flux during 1 year [*Tziperman*, 1986]. Here the function F is equivalent to the annual mean diapycnal volume flux.) The annual mean water mass transformation is a function only of the potential density. The double integral is the integral of the surface density flux $f(x, y, t)$ in the outcropping area where $\sigma_\theta = \sigma'_\theta$; δ is the delta function, where $\delta = 1$ if $\sigma_\theta = \sigma'_\theta$, otherwise $\delta = 0$. The surface density flux, $f(x, y, t)$ (kg m^{-2} s^{-1}), is defined as

$$f(x,y,t) = -\frac{\alpha H}{C_p} + \sigma_\theta(0,T)\frac{\beta(W \cdot S)}{1-S}. \tag{2}$$

In (2), $f(x, y, t)$ and all the other terms on the right hand side are functions of time and space; α and β are the thermal expansion and saline contraction coefficients ($\alpha = -\frac{\partial\rho}{\rho\partial T}$; $\beta = \frac{\partial\rho}{\rho\partial S}$); $\sigma_\theta(S, T)$ is the surface density; T and S are respectively the surface temperature and surface salinity; H is the heat flux and W is evaporation minus precipitation.

[18] From the area-integrated annual mean transformation function, it is possible to estimate the annual mean formation function [*Speer and Tziperman*, 1992; *Marshall et al.*, 1999],

$$\overline{M(\sigma_\theta)} = -\left[\overline{F(\sigma_\theta{}^{[2]})} - \overline{F(\sigma_\theta{}^{[1]})}\right], \tag{3}$$

where $\sigma_\theta^{[1]} < \sigma_\theta < \sigma_\theta^{[2]}$. $\overline{M(\sigma_\theta)}$ (m^3/s) is the annual mean formation (overbar is the time mean), i.e., the annual mean volume flux that accumulates (or is removed) between the isopycnals $\sigma_\theta^{[1]}$ and $\sigma_\theta^{[2]}$. In the limit of $\sigma_\theta^{[1]} \to \sigma_\theta^{[2]}$ (3) can also be written as $\delta\overline{M(\sigma_\theta)} = -\frac{\partial\overline{F}}{\partial\sigma}\delta\sigma$.

2.2.2. Computation

[19] Using the data described in section 2.1, we first computed the surface density flux $f_{i,j,k}$ (2). The subscripts i, j, represent the spatial grid points, while k refers to the time dimension. To reduce the uncertainties related to the discretization in time of the data, at each grid point the monthly values of the density flux $f(x, y, t)$ have been linearly interpolated in time, with a time step $\Delta t = 1.5$ days. (Shorter time steps tested on data subsets yielded the same results but with a major increase in computational cost.)

[20] Secondly, applying (1), we computed the annual mean transformation $\overline{F(\sigma_\theta)}$, hereinafter in units of *Sv* (1 *Sv* = 10^6 m^3/s), for densities $27.05\sigma_\theta$–$27.95\sigma_\theta$ in steps of $0.1\sigma_\theta$. These isopycnal densities outcrop in winter in our study domain (10°N–75°N, 100°W–20°E). This region extends well beyond the SPMW domain [*Brambilla and Talley*, 2008] because the formation calculation requires the full area of each isopycnal outcrop, including summertime. Values of $\overline{F(\sigma_\theta)}$ computed for the entire North Atlantic have been shown, using different data, in several previous studies [*Speer and Tziperman*, 1992; *Speer*, 1997; *Marshall et al.*, 1999; *Valdivieso Da Costa et al.*, 2005].

[21] Third, differently from the other papers, in addition to the space and time integral of the transformation function $\overline{F(\sigma_\theta)}$, we also show the regional distribution of the annual mean transformation function, $\overline{F(x, y, \sigma_\theta)}$ or $\overline{F_{i,j}(\sigma_\theta)}$ (Sv). (When the annual mean transformation function is integrated over the study domain, the (x, y) variables or the (i, j) indices are omitted.) The regional distribution $\overline{F(x, y, \sigma_\theta)}$ is computed as

$$\overline{F(x,y,\sigma_\theta)} \cong \overline{F_{i,j}(\sigma_\theta)} = \frac{1}{\Delta\sigma\Delta T}\sum_{k=1}^{240} \Delta t f_{i,j,k} A_{i,j} \Pi_{i,j}\left(\sigma_{\theta,i,j,k} - \sigma'_\theta\right), \tag{4}$$

where $f_{i,j,k}$ is the density flux at time k in the grid box (i, j). $A_{i,j}$ is the area of the corresponding grid box in which we are computing $\overline{F_{i,j}(\sigma_\theta)}$. $\Pi_{i,j,k}$ is the boxcar function; $\Pi_{i,j,k} = 1$ if $\sigma_{\theta,i,j,k}$ is equal to the outcrop density σ'_θ, $\Pi_{i,j,k} = 0$ otherwise. The time steps $\Delta t = 1.5$ days. The time period over which we compute the average is $\Delta T = 1$ year. The density bin width is $\Delta\sigma = 0.1$ kg/m^3.

[22] Fourth, using (3) we computed the annual mean water mass formation rate (Sv) integrated over the study domain. As noted in section 2.2.1, formation is the convergence of transformation between the two isopycnals $\sigma_\theta^{[1]}$ and $\sigma_\theta^{[2]}$, following usage common for Walin-type calculations [*Speer and Tziperman*, 1992]. Thus formation is the amount of water that is lost from the surface layer to the ocean interior if positive or the amount of water that obducts from the ocean interior if negative.

[23] Finally, it is useful to visualize the spatial distribution of formation as well as transformation. The definition of formation (3) eliminates any spatial information because it is based on spatial integrals of transformation. However, since formation is associated with density classes and these classes have well-defined outcrops, it is useful to visualize the spatial pattern of formation based on the outcropping regions. (Use of discrete estimates of the formation rate calculated at each grid point, computing the difference of the local transformation, has not been considered an adequate approach because this method is biased by the dependence of the transformation on the outcropping region. Transformation rates, by definition (1), are different from zero just in the outcropping region, thus the local difference is meaningful only if two different isopycnals

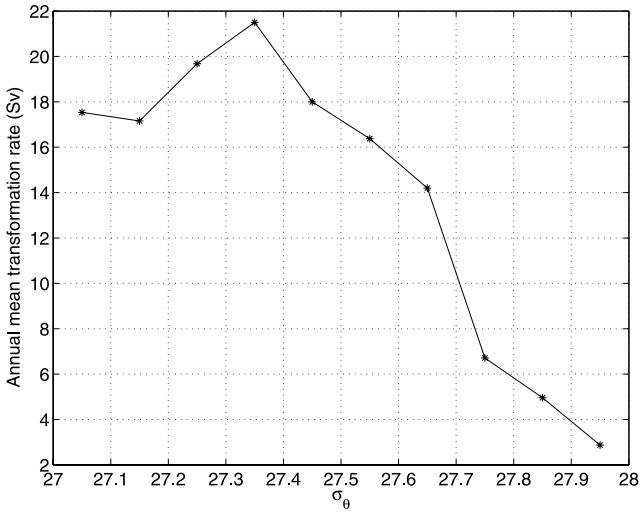

Figure 3. Annual mean transformation function $\overline{F(\sigma_\theta)}$ (Sv) that results from the spatial integral of the surface density flux over the study domain. The computation follows *Speer and Tziperman* [1992]. It spans density range $27.05\sigma_\theta$–$27.95\sigma_\theta$ with a density bin width of $\Delta\sigma_\theta$ = 0.1 kg/m^3.

outcrop at the same location and at the same time, which is impossible.)

[24] To visualize the spatial pattern of formation, we first compute the basin-integral transformation at each time step k,

$$M_k(\sigma'_\theta) = -\left[F_k\left(\sigma_\theta^{[2]}\right) - F_k\left(\sigma_\theta^{[1]}\right)\right], \tag{5}$$

where $F_k(\sigma_\theta^{[1],[2]})$ refers to the basin integral transformation values at time k for $\sigma_\theta^{[1],[2]}$ and $\sigma_\theta^{[1]} < \sigma'_\theta < \sigma_\theta^{[2]}$. Then, we identify the outcropping region ($R_k(\sigma'_\theta)$) for the isopycnal σ'_θ at time k. Hence, the instantaneous, but spatially averaged value of formation (subduction or obduction), (5) at each grid point in the outcropping region is

$$S_{i,j,k}(\sigma'_\theta) = \frac{M_k(\sigma_{\theta'})}{R_k(\sigma'_\theta)}, \qquad \forall\, i,j \quad \epsilon \quad R_k(\sigma'_\theta). \tag{6}$$

A map of annual formation (subduction and obduction) for each isopycnal σ'_θ is then obtained as the sum over the k time steps

$$\overline{S_{i,j}(\sigma'_\theta)} = \sum_{k=1}^{240} S_{i,j,k}(\sigma'_\theta) \tag{7}$$

in units of m/a.

3. Surface Water Mass Transformation

[25] *McCartney and Talley* [1982], updated by *Brambilla and Talley* [2008], showed that SPMWs dominate the layer between the ocean surface and the permanent pycnocline. This surface layer is obviously affected by the air-sea fluxes [*Walin*, 1982; *Speer and Tziperman*, 1992; *Marshall et al.*, 1999] that cause a diapycnal flux that primarily transforms SPMW from lower to higher densities.

[26] To estimate the diapycnal volume flux involved in the SPMW transformation and to identify the time and space frame in which SPMWs are transformed, we first show the estimates of the annual mean transformation function $\overline{F(\sigma_\theta)}$ for densities from $27.05\sigma_\theta$ to $27.95\sigma_\theta$. $\overline{F(\sigma_\theta)}$ is obtained from the integral of the surface density flux over the study domain (10°N–75°N, 100°W–20°E). Then, we provide maps of the regional distribution of the annual mean transformation function $\overline{F_{i,j}(\sigma_\theta)}$. Third, we discuss the time variability of the transformation estimates, again obtained from the spatial integral of the density flux over the study domain.

3.1. Annual Mean Transformation Rates

[27] The annual mean transformation function from the spatial integral over the study domain (Figure 3) is consistent and comparable with the geostrophic transport associated with the upper limb of the meridional overturning circulation [*McCartney and Talley*, 1984; *Krauss*, 1986; *Schmitz and McCartney*, 1993; *Schmitz*, 1995; *Ganachaud*, 2003; *Talley*, 2003], confirming that the diapycnal volume flux plays a dominant role in the shallow thermohaline transport [*Marsh*, 2000; *Lumpkin and Speer*, 2003]. The transformation varies from a minimum of 3 *Sv* crossing the $27.95\sigma_\theta$ isopycnal to a maximum of 21.5 *Sv* crossing the $27.35\sigma_\theta$ and has an average value of 14 ± 6.5 *Sv*. Thus, subpolar surface waters, which are dominated by SPMW, are being transformed at a rate that matches the transport by geostrophic currents across isopycnals. We then observe that the transformation (Figure 3) is characterized by increasing transport from $27.05\sigma_\theta$ to $27.35\sigma_\theta$ and decreasing transport from $27.35\sigma_\theta$ to $27.95\sigma_\theta$. This requires obduction from underlying denser waters into the $27.1\sigma_\theta$, $27.2\sigma_\theta$, and $27.3\sigma_\theta$ density classes. (The possible coexistence, at low density classes, of net obduction over the entire outcropping area and local subduction is discussed in section 4.1.) At higher surface density, the negative slope, usually interpreted as "subduction," is likely associated with loss through entrainment by deep overflows of the Irminger Sea and the Iceland Basin, rather than by upper ocean subduction of the sort found in the subtropics (see section 4.1).

[28] The transformation rates are consistent with previous studies. *Qiu and Huang* [1995], using Levitus climatology, observed a similar obduction peak for subtropical densities. In addition, similar trends for the basin integral of the annual mean transformation function were obtained by *Speer and Tziperman* [1992] using the *Isemer and Hasse* [1987] data set. However, since their data set did not extend to the Nordic Seas, they did not estimate annual mean transformation for the densest water masses. *Valdivieso Da Costa et al.* [2005], using model data output and applying a kinematic approach, obtained a similar behavior of the basin integral of the annual mean transformation function.

3.2. Regional Distribution of the Transformation Rates

[29] To identify the origin of SPMWs characterized by particular potential densities, the annual mean transformation function $\overline{F_{i,j}(\sigma_\theta)}$ is mapped on a regular $1^\circ \times 1^\circ$ grid (Figure 4). In order to track the geostrophic flow also involved in the transformation of one SPMW to another, and to illustrate the correspondence between SPMW locations and subpolar gyre currents as shown *Brambilla and*

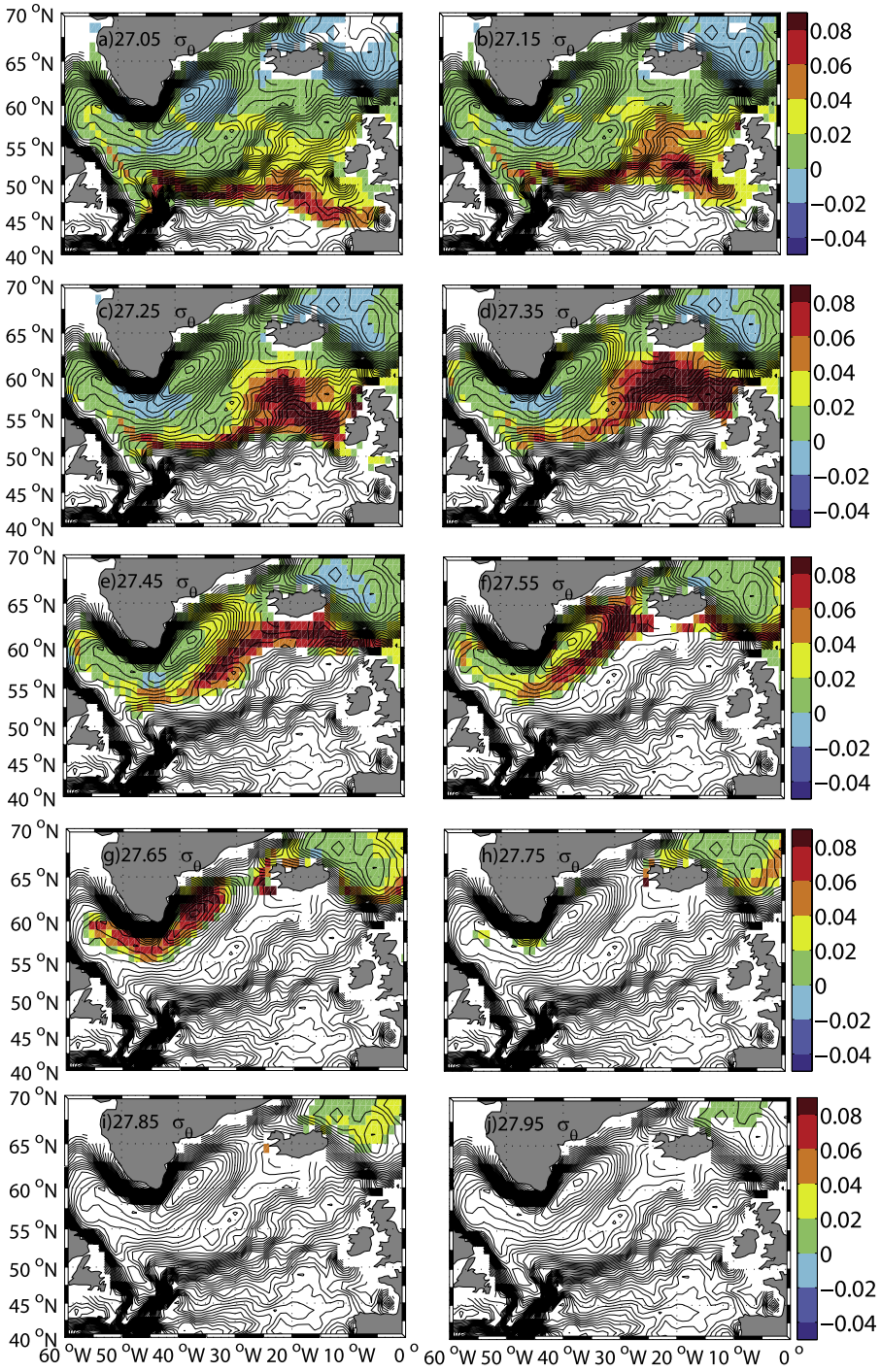

Figure 4. Regional distribution of the annual mean transformation function $\overline{F_{i,j}(\sigma_\theta)}$ (Sv). Values are plotted on a regular $1^\circ \times 1^\circ$ grid. The black lines are the surface flow streamlines with a contour interval of 2 m^2 s^{-2} from *Brambilla and Talley* [2008]. The computation extends over the entire study domain (10°N–75°N, 100°W–20°E). However, just the portion of the domain with significant results is shown. The white region in the southern part of each plot is due to lack of data because the corresponding isopycnal does not outcrop. Transformation across the isopycnals: (a) 27.05σ_θ, (b) 27.15σ_θ, (c) 27.25σ_θ, (d) 27.35σ_θ, (e) 27.45σ_θ, (f) 27.55σ_θ, (g) 27.65σ_θ, (h) 27.75σ_θ, (i) 27.85σ_θ, and (j) 27.95σ_θ.

Talley [2008], we superimpose the streamlines of the surface flow computed from surface drifters [*Brambilla and Talley*, 2008]. Each plot of Figure 4 shows where the surface water of a certain density σ_θ, outcropping at the surface, changes its density toward higher or lower values driven by the air-sea flux. The sum of the grid values of each plot of Figure 4 is equivalent to the integrated estimates shown in Figure 3.

[30] Positive (negative) values correspond to increasing (decreasing) of surface density, or in other words, to transformation toward increasing (decreasing) density.

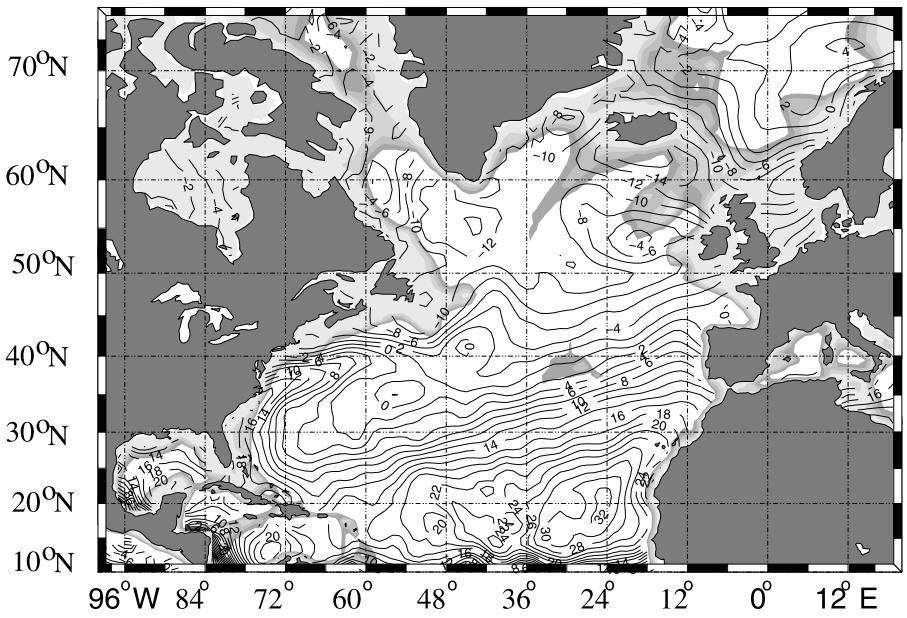

Figure 5. Annual mean buoyancy flux (kg m^{-1} s^{-3}) computed from the NOCS air-sea fluxes [*Grist and Josey*, 2003]. Bathymetry is shaded. Darkest contour is 2000 m, and lightest contour is 10 m. Contour interval is 500 m.

(Most of the transformation is associated with advection toward higher surface density.) In the computation of the transformation rate or diapycnal flux (1), it is impossible to distinguish between the change of surface water mass density that occurs locally as a result of an unsteady state, and that which involves actual movement of water through fixed isopycnals in condition of a steady state [*Speer and Tziperman*, 1992]. Here, since the transformation rates are annually averaged, the annual mean location of the outcropping isopycnals are fixed. Thus, the gradual northward progression of the transformation areas for greater densities suggests that the transformation involves mostly advection through outcropping isopycnals.

[31] Although each plot in Figure 4 is dominated by positive (red) annual mean transformation values, along the lightest isopycnals ($27.05\sigma_\theta$–$27.35\sigma_\theta$), there are also a few locations with negative (blue) transformation rates. These are mostly located south of Cape Farvel (Greenland), on the Iceland-Faroe Ridge and at a few grid points in the Irminger Sea. Each negative value is due to the imbalance between the local heating in spring-summer and the apparently weaker cooling that occurs in fall, which might suggest that these limited regions are characterized by a net positive buoyancy flux. However, the climatological buoyancy flux (Figure 5) is negative everywhere in the domain. Thus, we attribute the small ($O(10^{-2})$ Sv) negative transformation values to uncertainties related to the computational procedure; this in turn suggests an error in the calculation of ±0.02 Sv. (That is, in addition to the winter outcrop, light densities ($27.05\sigma_\theta$–$27.35\sigma_\theta$) outcrop also in summer at northern latitudes. At each grid location (i, j) the net transformation is the time integral of the negative density flux $f(x, y, t)$ (toward lighter density) in summer, and the positive density flux (toward greater density) in fall. However, since the ocean surface increases in density in fall more rapidly than in summer, the time discretization (dt = 1.5 days) causes an underestimate of the time integral for the fall period.)

[32] The location of largest diapycnal volume flux depends on the isopycnal, of course, and also follows the circulation tracked by the surface streamlines. The most intense transformations across the $27.05\sigma_\theta$, $27.15\sigma_\theta$, $27.25\sigma_\theta$, and $27.35\sigma_\theta$ isopycnals are located on the southern edge of the subpolar gyre and shift progressively northeastward in the Iceland Basin with increasing density (Figures 4a, 4b, 4c, and 4d). These regions are fed from the water coming from the eastward NAC, that subsequently splits into the Central Iceland Basin branch of the NAC and the Subarctic Front, that flow northeastward in the Iceland Basin [*Brambilla and Talley*, 2008], and the Rockall Trough branch of the NAC (Figures 4a, 4b, 4c, and 4d). The regions of most intense diapycnal volume flux across the $27.45\sigma_\theta$, $27.55\sigma_\theta$, $27.65\sigma_\theta$ isopycnals are located along the East Reykjanes Ridge Current, the Irminger Current and the East Greenland Current, and in the Nordic Seas along the Norwegian Current (Figures 4e, 4f, and 4g).

[33] Looking at each NAC branch, the region of intensified transformation proceeds downstream from lower to higher density. This is consistent with the progression of SPMW density along each current, as shown by *Brambilla and Talley* [2008].

[34] The Labrador Sea, Irminger Sea and Nordic Seas are characterized by intense diapycnal flux across the $27.65\sigma_\theta$ isopycnal (Figure 4g), consistent with dense water formation [e.g., *Pickart et al.*, 2003]. This is further explored in section 4.

[35] The regions of intense water mass transformation are associated with SPMW, identified by the minimum of potential vorticity along specific isopycnals ($27.3\sigma_\theta$, $27.4\sigma_\theta$, $27.5\sigma_\theta$, Figure 6). Integrating the transformation rates across the $27.25\sigma_\theta$, $27.35\sigma_\theta$, $27.45\sigma_\theta$ isopycnals in the areas identified by the contours of low potential vorticity,

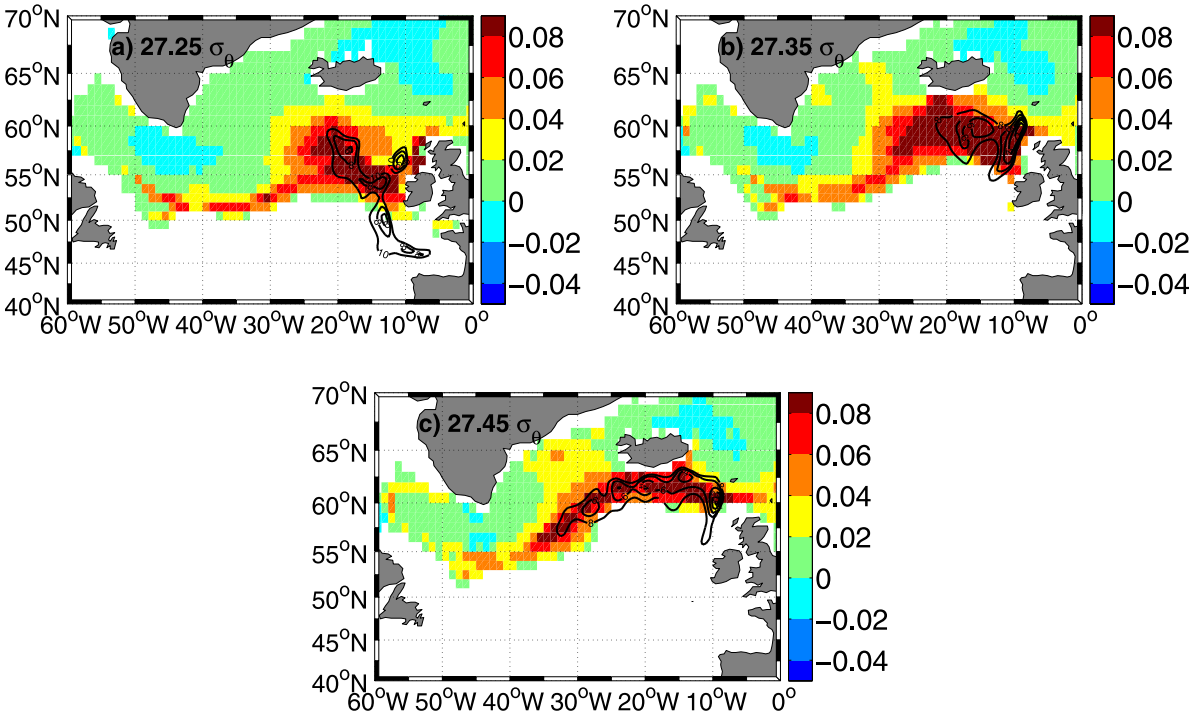

Figure 6. Regional distribution of the annual mean transformation function $\overline{F_{i,j}(\sigma_\theta)}$ (Sv) plotted on a regular $1^\circ \times 1^\circ$ grid, as in Figure 4. (a) Transformation across the $27.25\sigma_\theta$ isopycnal. The black contours represent the minimum of potential vorticity computed on the $27.3\sigma_\theta$ isopycnal. The PV varies from 0 to 10×10^{-13} cm^{-1} s^{-1}. Contour interval is 2×10^{-13} cm^{-1} s^{-1}. (b) Transformation across the $27.35\sigma_\theta$ isopycnal. The black contours represent the minimum of potential vorticity computed on the $27.4\sigma_\theta$ isopycnal. The PV varies from 0 to 8×10^{-13} cm^{-1} s^{-1}. Contour interval is 2×10^{-13} cm^{-1} s^{-1}. (c) Transformation across the $27.45\sigma_\theta$ isopycnal. The black contours represent the minimum of potential vorticity computed on the $27.5\sigma_\theta$ isopycnal. The PV varies from 0 to 8×10^{-13} cm^{-1} s^{-1}. Contour interval is 2×10^{-13} cm^{-1} s^{-1}.

we find a throughput of the $27.3\sigma_\theta$ and $27.4\sigma_\theta$ SPMW of ~6 Sv and a throughput of the $27.5\sigma_\theta$ SPMW of ~8 Sv. These values are relatively small (~30%) with respect to the spatially integrated transformation rate over the entire isopycnal outcropping region for the same densities (~19.5 *Sv* across $27.25\sigma_\theta$; ~21.5 Sv across $27.35\sigma_\theta$; ~18 Sv across $27.45\sigma_\theta$, Figure 3). However, if the SPMW throughput (transformation of the water masses with low PV) is compared to the spatial integral of the transformation rate limited to the areas of largest values (darkest squares in Figures 6a, 6b, and 6c), a better agreement is found. Integrating the regional distribution of the transformation rate only in the region where the local transformation is larger than 0.05 Sv (therefore, summing only the grid boxes where $\overline{F}_{i,j}(\sigma_\theta) > 0.05$ Sv), we obtain the following transformation values: ~10 Sv across $27.25\sigma_\theta$; ~12 Sv across $27.35\sigma_\theta$; ~8 Sv $27.45\sigma_\theta$. These estimates are close to the SPMW throughput estimates (transformation of water masses with low PV, as shown earlier in this section); thus it can be hypothesized that the surface water masses transformed by air-sea interaction are mainly associated with SPMW, and that air-sea interaction is necessary for SPMW transformation. At $27.3\sigma_\theta$ and $27.4\sigma_\theta$, the discrepancies between the SPMW throughput and the rate of transformation integrated over regions where transformation is large might be due to the uncertainties in the definition of the areas occupied by SPMW in the corresponding density classes, which depend highly on the availability of the hydrographic stations [*Brambilla and Talley*, 2008]. Hence, it is appropriate to suggest that SPMW is a major component of the shallow limb of the overturning circulation, but it does not constitute all of it.

3.3. Temporal Variability

[36] The regional distribution of the transformation function (Figure 6) showed the spatial correspondence between transformation and the more limited location of SPMW of the same densities. Here, we investigate the temporal variability of the transformation function, using the basin integrated transformation function computed at each time step (Figure 7). The temporal variability of transformation has been shown in previous studies [e.g., *Speer and Tziperman*, 1992; *Valdivieso Da Costa et al.*, 2005]. However given the different data and the focus on specific isopycnals in our study, this brief analysis useful to complete the discussion of SPMW transformation.

[37] In Figure 7, the sum of the time series of the estimated transformation rates corresponds to the annual transformation shown in Figure 3. Positive transformations (toward higher density) occur in winter and fall when heat is lost from the ocean to the atmosphere; negative transforma-

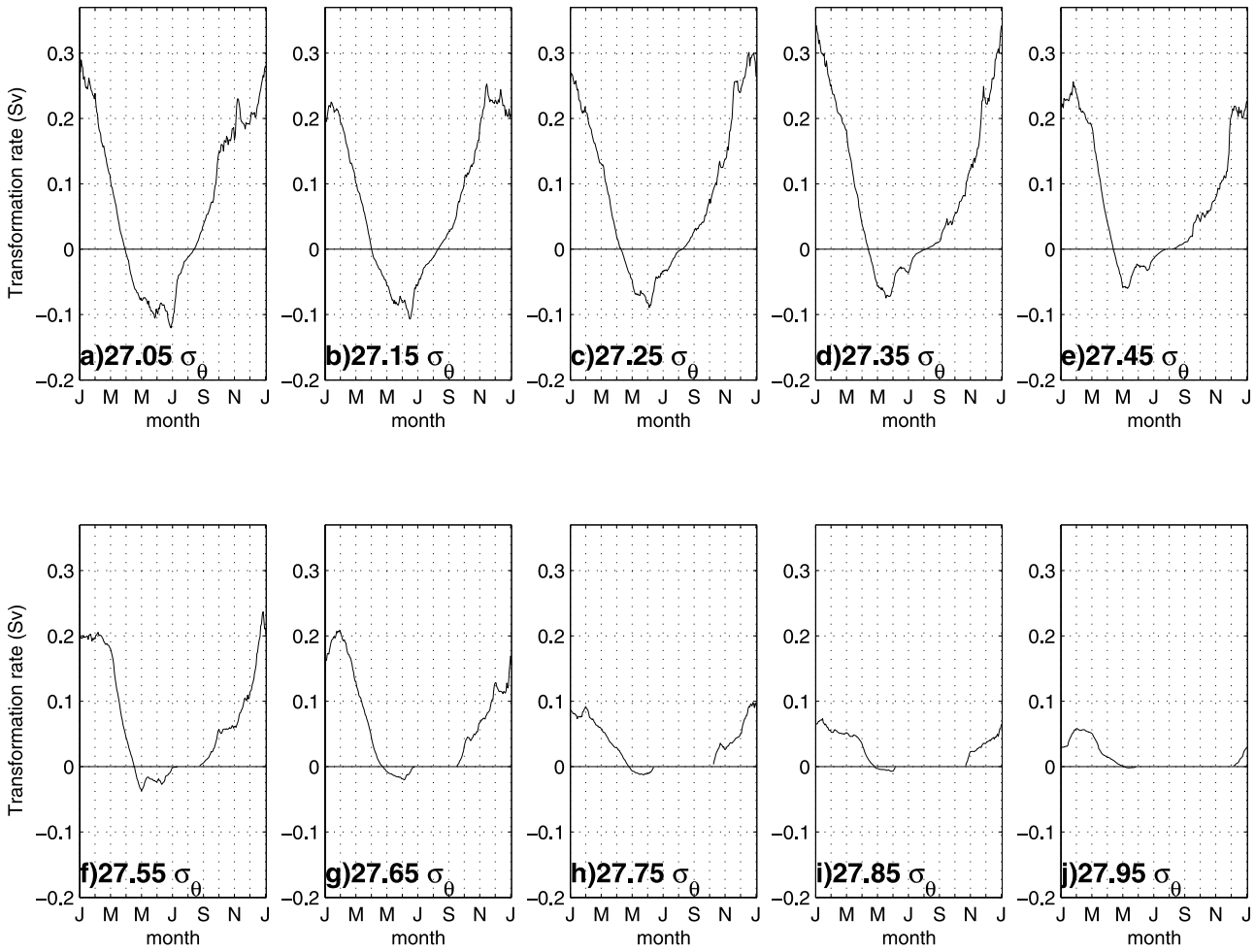

Figure 7. Time series of the transformation function (Sv) integrated over the study domain computed for each time dt = 1.5 days. (a) 27.05σ_θ, (b) 27.15σ_θ, (c) 27.25σ_θ, (d) 27.35σ_θ, (e) 27.45σ_θ, (f) 27.55σ_θ, (g) 27.65σ_θ, (h) 27.75σ_θ, (i) 27.85σ_θ, and (j) 27.95σ_θ. Positive values correspond to buoyancy loss, and negative values correspond to buoyancy gain.

tions (toward lighter densities) occur in late spring and summer, when heat is gained by the ocean.

[38] The transformation that occurs during the cold months is associated with deep mixed layers and hence SPMW. In late fall, the mixed layer starts deepening and summer stratification tends to disappear. The isopycnal layer that outcrops at the surface is affected by the heat lost from the ocean to the atmosphere and is eventually transformed to another surface water mass of higher density. The new surface water mass is characterized by nearly uniform properties and corresponds to new SPMW. Thus, winter transformation dominates the diapycnal flux that creates SPMWs, as suggested by *McCartney and Talley* [1982].

[39] The negative monthly values of water mass transformation (from dense to light densities) are due to the summer warming and restratification. Lighter densities (27.05σ_θ to 27.45σ_θ) are present at the surface in summer at more northern latitudes ($\sim$60°N) than the winter outcrop; the denser isopycnals ($\sigma_\theta > 27.45$) outcrop just in winter in our study domain. For this reason, the negative values of the transformation rates are larger at lighter densities (Figures 7a, 7b, 7c, 7d, and 7e) and smaller for higher density classes (Figures 7f, 7g, 7h, 7i, and 7j).

4. SPMW Formation

[40] The basin-integrated annual mean water mass transformation (Figure 3) is the rate at which surface water masses change density owing to air-sea fluxes. If the rates were constant for all the density classes considered, we could conclude that the densest surface water mass originates, through transformation, from the lightest surface water mass in complete isolation from exchange with the ocean interior (as summarized later by Figure 10a). The same process also describes the density progression of SPMWs, since these are part of the subpolar gyre surface layer. However, the transformation rate is not constant. This requires convergence or divergence, leading to positive or negative formation (subduction or obduction) of surface water masses that thus can affect the transport of SPMW.

[41] We first estimate the volume of the surface layer of each density class that is formed annually (subducted or obducted), by taking the difference between the basin integral of the annual mean transformation function at two

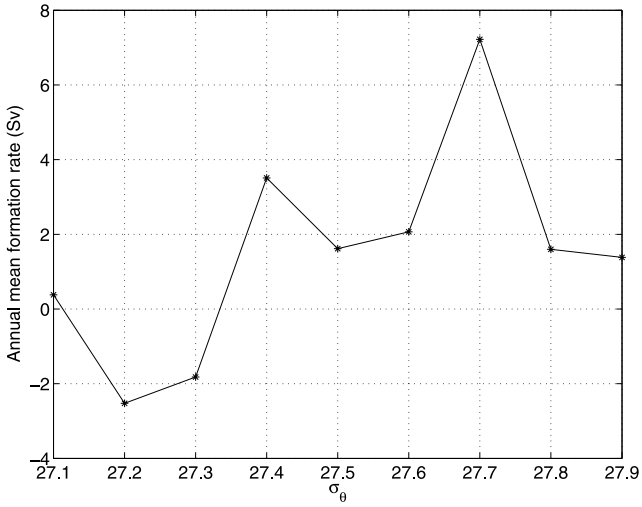

Figure 8. Annual mean formation (subduction/obduction) rate (Sv) resulting from the spatial integral over the study domain. The computation follows *Speer and Tziperman* [1992].

subsequent isopycnals. Secondly, we qualitatively map formation in the $27.3\sigma_\theta$, $27.4\sigma_\theta$, $27.5\sigma_\theta$ isopycnal layers using the method described in section 2.2. By superimposing the absolute stream function of the corresponding isopycnal flow [from *Brambilla and Talley*, 2008] on the formation map, it is possible to identify the paths followed by subducted/obducted surface water. The comparison with observations of SPMW obtained using hydrographic data [*Brambilla and Talley*, 2008] will be useful to interpret our results.

4.1. Annual Mean Formation Rates

[42] The difference between the basin-integrated annual mean transformation rates at two subsequent isopycnals (Figure 8) provides a rough approximation of the annual net positive or negative formation of the surface water masses [*Speer and Tziperman*, 1992; *Nurser et al.*, 1999; *Valdivieso Da Costa et al.*, 2005]. Annual net negative formation (obduction) occurs at light densities, ~ -2.5 Sv at $27.2\sigma_\theta$ and ~ -2 Sv at $27.3\sigma_\theta$, suggesting net obduction into the mixed layer. On the other hand, *McCartney and Talley* [1982], *McCartney* [1982], and *Paillet and Arhan* [1996] showed subduction in the eastern subtropical gyre for these light density classes, $27.0 < \sigma_\theta < 27.3$, based on maps of isopycnal properties; these outcrops are in a net Ekman downwelling region, which therefore yields net wind-driven subduction, not obduction. Apparently net obduction over the entire isopycnal outcrop region is not incompatible with regional subduction [*Marshall et al.*, 1993].

[43] As opposed to the obduction observed at lower densities, positive annual net water mass formation ("subduction") occurs at densities greater than $27.35\sigma_\theta$, suggesting that water transfers from the mixed layer to the ocean interior. The positive formation (subduction) values for the $27.4\sigma_\theta$, $27.5\sigma_\theta$, $27.6\sigma_\theta$ surface water masses are likely associated with turbulent entrainment of warm water into the deep overflows in both the Irminger Sea and the Iceland Basin, rather than with the classical subduction of subtropical gyres. This interpretation is driven by the conclusion of the accompanying paper [*Brambilla and Talley*, 2008] that low potential vorticity SPMW does not move into the interior along isopycnals in the subpolar gyre, despite the calculated net convergence of transformation. Hence, the positive formation ("subduction") is likely due to entrainment by deeper and denser flow, therefore losing characteristic properties such as low potential vorticity.

[44] Supporting this interpretation, in situ observations of the entrainment flux in the eastern subpolar gyre and the formation rates roughly agree. South of Iceland, [*Steele et al.*, 1962] measured deep southwestward transport on the order of 5 Sv choosing a level of no motion based on the T-S values. They pointed out that just 1.4 to 2 Sv of these 5 Sv was actual Nordic Seas overflow water, while the rest was due to entrainment of Atlantic water. Another estimate of the overflow flux was obtained by [*Saunders*, 1996], who, using mooring measurements lasting 1 year, estimated that the transport south of Iceland, at $\sigma_\theta \geq 27.8$, has a mean value of 3.2 Sv with a standard deviation of 1.4 Sv. Of this, $\sim$1.5 Sv are Norwegian Sea water. Thus, the $\sim$3.5 Sv formation of the water mass at $27.4\sigma_\theta$ that we compute is comparable with the upper limit of the observed entrainment rate. (The deeper Labrador Sea Water is likely also entrained.) Analogously, in the Irminger Sea, *Dickson and Brown* [1994] estimated that the $\sim$3 Sv of Denmark Overflow Water (DOW) transport increases up to $\sim$5 Sv in the first 160 km owing to warm entrainment. Our formation rates on the order of 2 Sv for the $27.5\sigma_\theta$ and the $27.6\sigma_\theta$ SPMWs are comparable.

[45] The larger positive formation rate obtained for the $27.7\sigma_\theta$ surface layer is also entrained in the dense flow that then participates in the formation of the Labrador Sea Water (LSW). The formation area of the $27.7\sigma_\theta$ water mass in the Irminger Sea (Figure 4g) is in agreement with the recent results from *Pickart et al.* [2003].

4.2. Regional Distribution of the Formation (Subduction/Obduction) Estimates

[46] As explained in section 2.2, associating the annual formation (subduction/obduction) rates integrated over the entire study domain with the corresponding outcropping areas, we have been able to roughly represent the main regions and the spatially-averaged magnitude of the formation values on various isopycnal layers (as described in section 2.2). (As noted above, "subduction" is equivalent to positive "formation," but in this Ekman-upwelling subpolar region is not synonymous with the wind-forced downwelling of subtropical gyres.) However, it should be noted that since the method is based on atmospheric data and not on direct observation of the vertical flux across the permanent pycnocline, the formation distribution maps shown here refer to processes that take place in the upper mixed layer. Therefore these maps do not identify the areas where the water is actually transferred across the permanent pycnocline. Advection within the mixed layer causes displacement between the formation (subduction/obduction) regions in the mixed layer and the exchange regions through the permanent pycnocline.

[47] The isopycnal layer centered around $27.3\sigma_\theta$ (Figure 9a) is characterized by relatively strong divergence

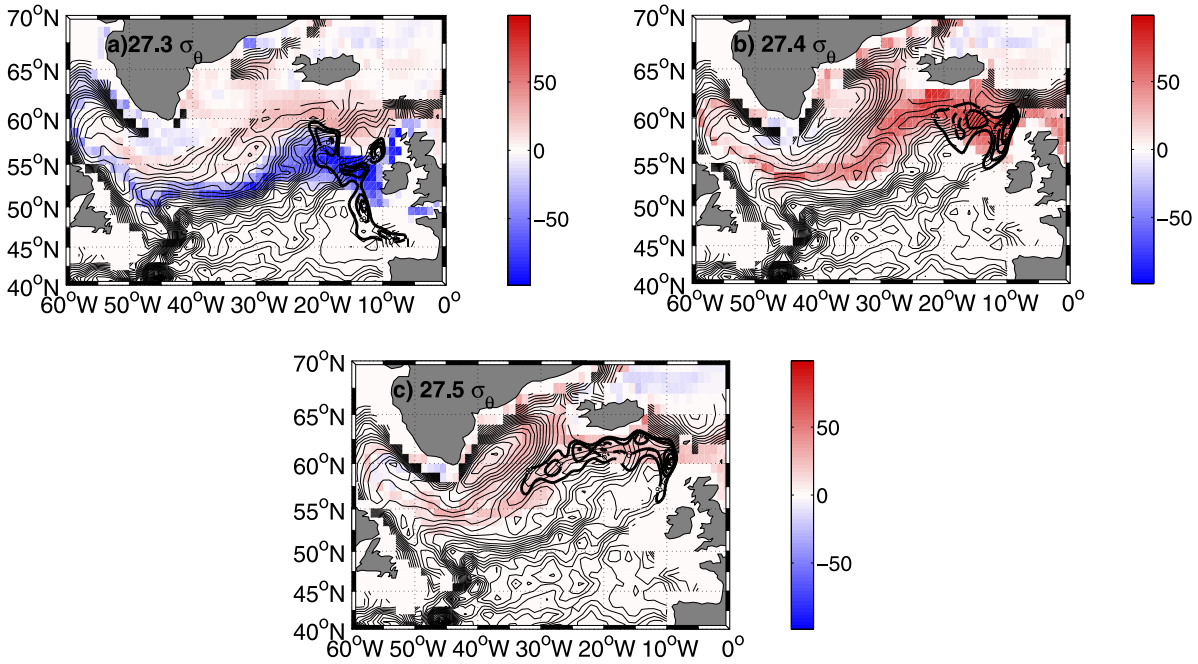

Figure 9. Annual mean formation (subduction/obduction) rates (m/a) $\overline{S_{i,j}}$ plotted on a $1^\circ \times 1^\circ$ regular grid. Positive values (red) correspond to annual mean positive formation (subduction), and negative values (blue) correspond to annual mean negative formation (obduction). The formation regions do not necessarily coincide with the places where exchange of surface water through the permanent pycnocline takes place because of advection within the mixed layer. (a) $\overline{S_{i,j}(27.3\sigma_\theta)}$ and the stream function on the $27.3\sigma_\theta$ isopycnal. (b) $\overline{S_{i,j}(27.4\sigma_\theta)}$ and the stream function on the $27.4\sigma_\theta$ isopycnal. (c) $\overline{S_{i,j}(27.5\sigma_\theta)}$ and the stream function on the $27.5\sigma_\theta$ isopycnal. Stream functions are based on a surface drifter velocity reference and geostrophic shear from climatological hydrographic data [from *Brambilla and Talley*, 2008]. Heavy black contours refer to the areas of low potential vorticity that identify SPMWs, as in Figure 6.

in the southern part of the subpolar gyre, following the northeastward flow of the NAC branches. This suggests that water from the ocean interior upwells into the mixed layer to replenish the loss of $27.3\sigma_\theta$ water mass. Hence, the $27.3\sigma_\theta$ water that is eventually transformed into the $27.4\sigma_\theta$ water mass is not just part of the mixed layer but is diluted with water from the interior. Most of the divergence occurs along the main NAC and along the southern side of the Rockall Trough and Iceland Basin branches of the NAC.

[48] The region of positive formation north of the obduction area, in Figure 9a, is a combined effect of the method applied to obtain the regional distribution of formation (subduction/obduction) values and the summer restratification that results in a northward shift of the outcropping region. The positive value of formation is caused by the larger negative transformation (toward lower densities, Figure 7) across the $27.25\sigma_\theta$ than that across the $27.35\sigma_\theta$, integrated over the study domain, in late spring and summer due to the progressive warming of the surface layer. Here, as explained in section 2.2, the formation (subduction/obduction) rate integrated over the study domain at a fixed time (t) is associated with the outcropping area at the corresponding time. Moreover, the outcropping area shifts northward in the warm months. Therefore, although we present the regional distribution of formation rates averaged over 1 year, it is possible to identify an area of positive formation that occurs only during the warm season.

[49] The formation (subduction/obduction) maps along the $27.4\sigma_\theta$ and $27.5\sigma_\theta$ isopycnal layers (Figures 9b and 9c) differ significantly from the $27.3\sigma_\theta$ isopycnal. Both the $27.4\sigma_\theta$ and $27.5\sigma_\theta$ isopycnals are dominated by positive formation. The positive formation values on the $27.4\sigma_\theta$ isopycnal are larger than on the $27.5\sigma_\theta$ isopycnal.

[50] Because of the limitation of these maps, which cannot capture advection, the positive formation areas of the $27.4\sigma_\theta$ and $27.5\sigma_\theta$ maps most likely do not coincide with the locations of loss through the pycnocline. Nevertheless, the absolute stream functions on the $27.4\sigma_\theta$ and $27.5\sigma_\theta$ isopycnals clearly illustrate the path followed by the newly formed water masses (Figures 9b and 9c) (although this information will not be used to track subducted SPMW since we interpret SPMW subduction as entrainment into subpolar gyre deep flow, see section 4.1). The $27.4\sigma_\theta$ water mass follows the Central Iceland Basin branch of the NAC and the Subarctic Front [*Brambilla and Talley*, 2008] at the northern side of the Iceland Basin, and the East Reykjanes Ridge Current along the eastern flank of the Reykjanes Ridge. The $27.5\sigma_\theta$ water mass seems to follow the Central Iceland Basin branch of the NAC and the Subarctic Front just before joining the Iceland-Faroe Front. It also follows the East Reykjanes Ridge Current and the Irminger Current.

[51] In order to identify the part of the surface layer constituted by SPMW, the area of low potential vorticity corresponding to SPMW is superimposed on the formation

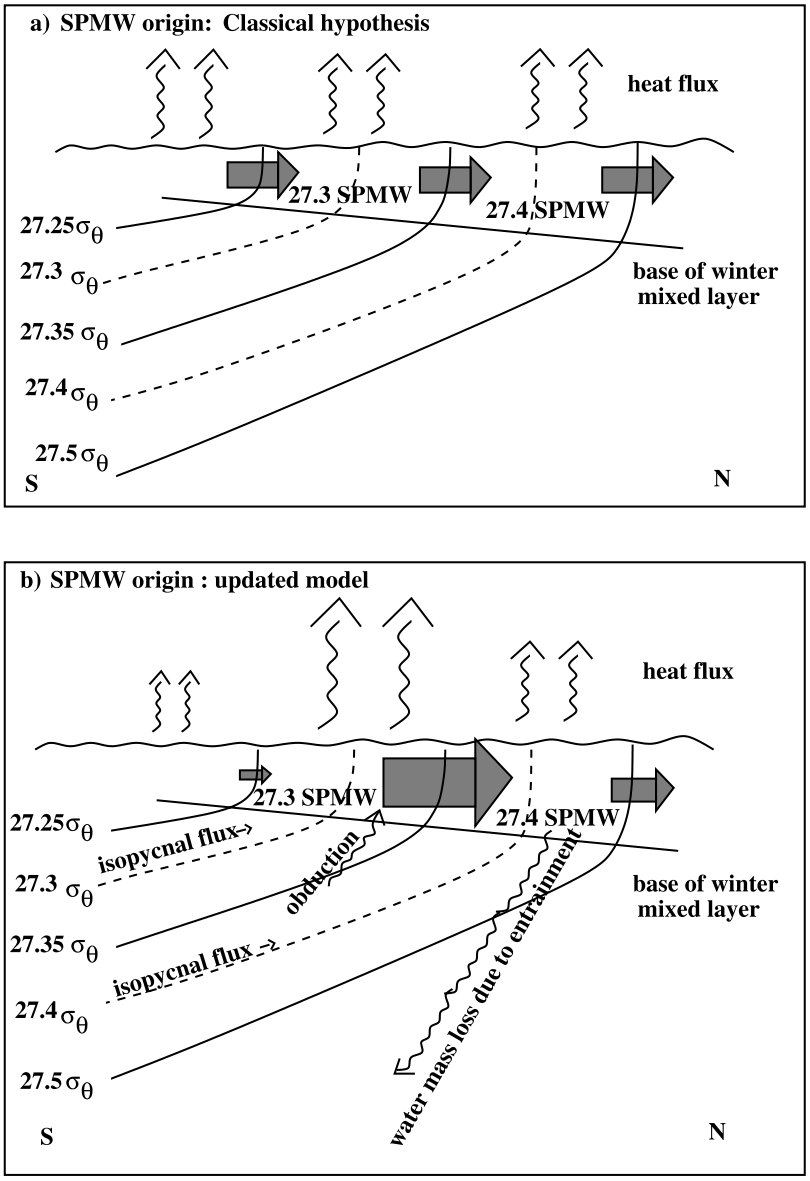

Figure 10. Schematics summarizing the processes that create SPMWs. (a) If the instantaneous transformation across subsequent isopycnals is constant (in terms of rate), the surface water mass with a certain density is the source for the surface water mass with greater density, and results from transformation of the surface water mass. This process occurs with no water mass exchange with the ocean interior. (b) If the instantaneous transformation across subsequent isopycnals is not constant (in terms of rate), it leads either to a deficit of surface water (e.g., at $27.3\sigma_\theta$) that requires obduction from the ocean interior, or to accumulation of surface water (e.g., at $27.4\sigma_\theta$) that drives subduction into the ocean interior. In the latter case, since it has been observed that SPMW does not subduct in the ocean interior [*Brambilla and Talley*, 2008] the loss of surface water is interpreted as entrainment by the deep flows of the subpolar gyre.

maps for the $27.3\sigma_\theta$, $27.4\sigma_\theta$, and $27.5\sigma_\theta$ water masses (Figure 9). Similarly to the ratio between the transformation regions and SPMW areas (section 3.2), also here, SPMWs occupy reduced ($\sim$1/3) regions with respect to where positive and negative formations occur (heavy contours on each plot of Figure 9 represent the low potential vorticity, i.e., the SPMW areas).

[52] Thus, we have observed that along the advection paths of each surface water mass considered, not all the water transformed into a certain water mass density is subsequently transformed into a further denser one. Therefore, since SPMW is part of the surface layer, not all the water added to a denser SPMW was transformed from the predecessor SPMW (Figure 10b).

[53] The maps shown in Figure 9 cannot be directly compared with the subduction/obduction estimates at the base of the winter mixed layer computed by *Marshall et al.* [1993] and *Qiu and Huang* [1995]. Here, in fact, we are computing the average (subduction/obduction) in isopycnal layers represented by their winter outcrop regions. On the

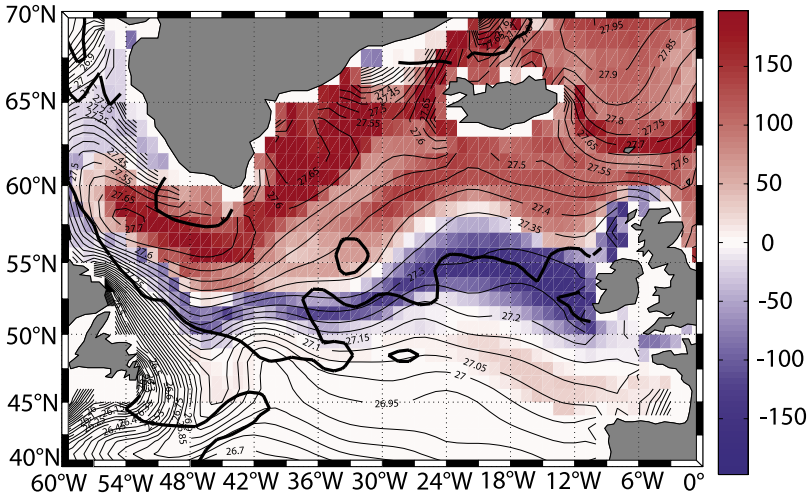

Figure 11. Annual mean formation (subduction/obduction) rates (m/a) for densities $27.05\sigma_\theta - 27.95\sigma_\theta$ plotted on a $1^\circ \times 1^\circ$ regular grid. Positive values correspond to annual mean subduction, negative values correspond to annual mean obduction. Black thick contour is the zero wind stress curl from the NOCS climatology. North of the thick black contour, the wind stress curl is positive; south of it, it is negative. Thin contours are the surface density from WOA01 climatology for March, Contour interval is 0.05 kg/m^3. No formation values are calculated for densities lighter than $27.05\sigma_\theta$ or greater than $27.95\sigma_\theta$.

other hand, the sum of the formation estimates for all the outcropping isopycnal layers considered, at each grid point, might be interpreted as the subduction/obduction that occurs at the subpolar gyre surface, hence, it can be compared with work by *Marshall et al.* [1993] and *Qiu and Huang* [1995].

[54] Figure 11 shows the result of our exercise. The region south of ~55°N is characterized by divergence, consistent with the obduction shown by *Marshall et al.* [1993] and *Qiu and Huang* [1995]. On the other hand, differing from their results, north of ~55°N the subpolar gyre is characterized by formation. This result apparently contradicts the expected upwelling due to the positive wind-stress curl and present in the subpolar North Atlantic. To the north the wind stress curl is positive and to the south it is negative, resulting in Ekman suction and pumping, respectively, which should drive obduction and subduction in these regions. These processes are further enhanced by lateral induction which leads to horizontal advection into the mixed layer in the area of positive wind stress curl, and lateral advection into the thermocline in the region of negative wind stress curl [*Marshall et al.*, 1993]. However, as mentioned in section 4.1, positive formation resulting from the convergence of transformation is likely associated with mass loss by entrainment, and not with classical subduction. (This highlights the difficulty with nomenclature. When obduction and subduction are defined on the basis of air-sea fluxes, they lose their simple, original definitions based on the sign of Ekman pumping.)

[55] The major obduction region on this map is closely associated with the zero wind-stress curl. The least dense subpolar surface water is in the wind-driven obduction region and far enough from the northern sill that its mass balance is mainly affected by the wind. In contrast, the higher-density surface water farther north, which is subject to wind driven obduction, actually loses mass, likely through entrainment.

[56] The surface density contours in March are also superimposed on Figure 11. The $27.35\sigma_\theta$ isopycnal coincides with the boundary between the formation and obduction regions by definition, because of the way that the maps were constructed from the basin-integrated transformations of Figure 3.

5. Isopycnal Flux Estimates

[57] We showed in section 3 that the diapycnal volume flux driven by air-sea interaction causes the transformation of SPMW density. However, diapycnal volume flux might not be the only source of SPMW. Hence, we need to estimate the isopycnal flux contribution to SPMW. This consists of subsurface water on a given SPMW isopycnal that enters the SPMW region from the south and then joins the layer of newly formed SPMW that results from diapycnal transformation of less dense SPMW.

[58] To estimate the isopycnal flux, we compute the baroclinic component of the geostrophic transport across the A24 WOCE hydrographic section from 1997 that crosses the eastern North Atlantic subpolar gyre from Greenland to Scotland, concentrating on the SPMW layer (Figure 12a). The geostrophic transport is computed as a function of the potential density. The water column is divided in 29 layers between $27.25\sigma_\theta$ and $27.975\sigma_\theta$. Each layer has a constant density width of 0.025 kg/m^3. To these we add the upper layer between the ocean surface and the $27.25\sigma_\theta$ isopycnal. We have not carried out a full analysis of reference velocities for the geostrophic flow. We find that by examining results from a range of choices of a level of no motion, we obtain enough information to constrain our estimate of isopycnal transport.

[59] Geostrophic transport with a level of no motion at 800 m (approximately 27.65 σ_θ) is shown for illustration in Figure 12b. This choice allows a correct resolution of the dense water transport, which is southward and roughly

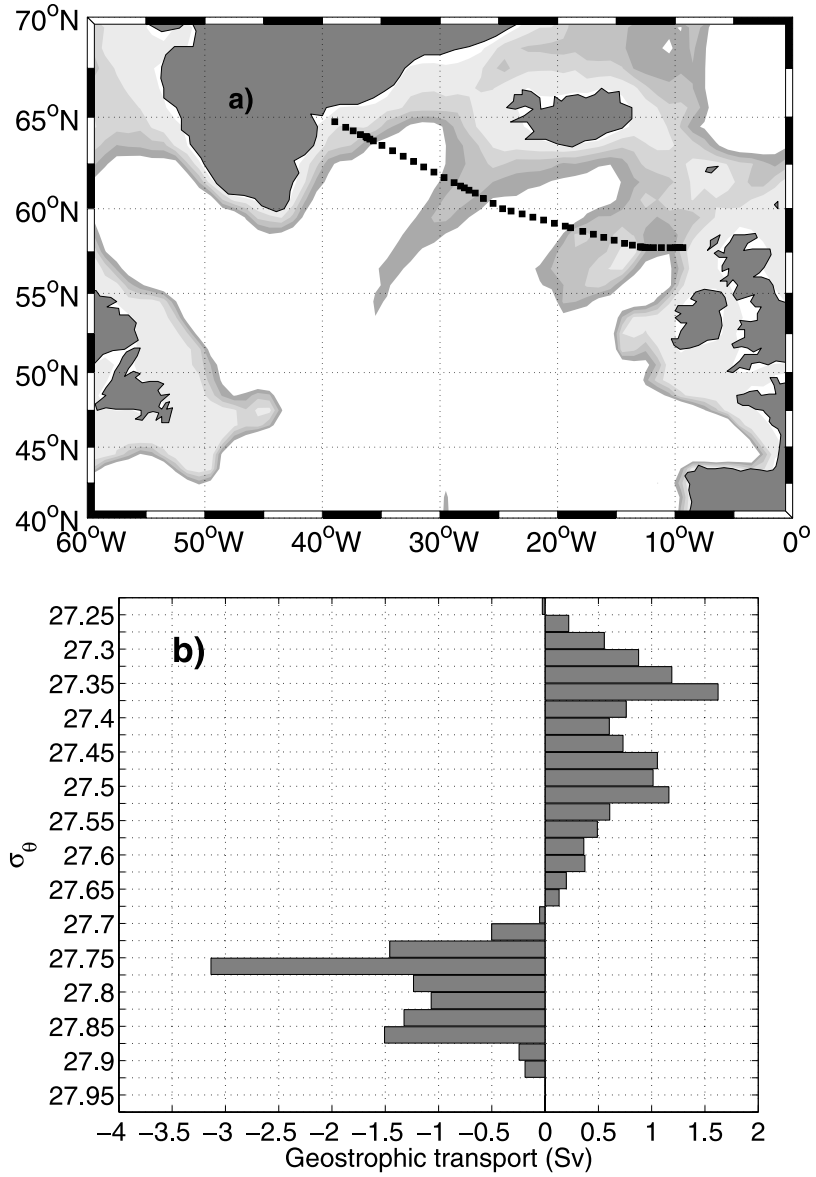

Figure 12. Geostrophic transport (Sv) measured across the A24 WOCE section. (a) Location of the transect. Bathymetry is shaded. Darkest contour is 2000 m, and lightest contour is 10 m. Contour interval is 500 m. (b) Geostrophic transport with level of no motion at 800 m (approximately $27.65\sigma_\theta$).

balances the northward flow. (The total transport across the section with this choice is ~1 Sv.) The real flow across this section likely has significant barotropic structure coupled with bottom-intensified, southward overflow. Despite the unrealistic level of no motion, this calculation is useful to describe the features of the shallow flow, characterized by two peaks of northward transport centered around $27.35\sigma_\theta$ and $27.475\sigma_\theta$. A different choice of level of no motion, although affecting the structure of the dense flow ($\sigma_\theta > 27.675$) and the net transport, does not cause any significant change in this shallow structure.

[60] The transport associated with each of these peaks varies from a minimum on the order of 3 Sv, obtained with a level of no motion at 800 m, to a maximum on the order of 8 Sv, obtained with a level of no motion at the bottom (not shown). These values represent 10%–40% of the basin-integrated diapycnal flux, thus suggesting that the diapycnal flux dominates SPMW transformation, and that the isopycnal flux is less than half of the diapycnal component.

6. Summary and Conclusions

[61] SPMWs are the thick surface water masses of the subpolar North Atlantic. Thus, they are an important part of the surface layer affected by air-sea interaction. Therefore, we have considered it useful to study the relation of SPMWs to transformation of the surface water masses as described by *Walin* [1982] and *Speer and Tziperman* [1992]. Different from the many previous studies of North Atlantic water mass transformation [*Tziperman*, 1986; *Garrett et al.*, 1995; *Garrett and Tandon*, 1997; *Nurser et al.*, 1999; *Marsh*, 2000; *Speer and Tziperman*, 1992; *Speer et al.*, 1995; *Speer*, 1997; *Marshall et al.*, 1999; *Gulev et al.*, 2003; *Valdivieso Da Costa et al.*, 2005], we have presented the regional

distribution of the annual mean transformation function on isopycnals, to localize the regions where surface layers, including SPMWs, of various densities are transformed.

[62] Our estimates of the basin-integrated annual mean transformation, in agreement with previous studies and the transport of the upper limb of the meridional overturning circulation [*McCartney and Talley*, 1984; *Krauss*, 1986; *Speer and Tziperman*, 1992; *Schmitz and McCartney*, 1993; *Schmitz*, 1995; *Ganachaud*, 2003; *Talley*, 2003], vary from 21.5 Sv at $27.35\sigma_\theta$ to 3 Sv at $27.95\sigma_\theta$. The average is 14 ± 6.5 Sv. The regional distribution of the annual mean transformation function shows a very good correspondence between the intense transformation regions across $27.25\sigma_\theta$, $27.35\sigma_\theta$, and $27.45\sigma_\theta$ and the locations of the $27.3\sigma_\theta$, $27.4\sigma_\theta$, and $27.5\sigma_\theta$ SPMWs, identified as regions with low potential vorticity. We observed that SPMW regions are not as extensive as the transformation regions. SPMW throughput is $\sim$30% of the transformation rate spatially integrated over the entire isopycnal outcrop regions. However, we have also shown that the SPMW throughput is in better agreement with the transformation rate, if the latter is integrated only in the region with the largest values ($\overline{F}_{i,j} >$ 0.05 Sv). Applying this constraint, we found that the diapycnal flux is $\sim$10 Sv across the $27.25\sigma_\theta$, $\sim$12 Sv across the $27.35\sigma_\theta$, and $\sim$8 Sv across the $27.45\sigma_\theta$. Thus, SPMWs can be interpreted as the link between the warm and salty water from the subtropical gyre and the dense water formed in the Labrador Sea and the Nordic Seas [e.g., *McCartney and Talley*, 1982, 1984; *Schmitz and McCartney*, 1993; *McCartney and Mauritzen*, 2001], but they do not constitute the entire transport of the shallow overturning circulation.

[63] In addition, analysis of the time series of the basin integrated transformation rates shows that the period from late fall through winter is characterized by the maximum transformation values. Thus, we confirm that most of the diapycnal flux that creates the SPMWs occurs in winter, as suggested by *McCartney and Talley* [1982].

[64] The smooth density progression of the surface water masses transformed by air-sea flux confirms that a certain SPMW characterized by a specific density can be generally interpreted as the source and the predecessor of denser and lighter SPMW, in agreement with *McCartney and Talley* [1982]. However, important constraints should be added to this statement, as follows.

[65] 1. The source/product chain for SPMW transformation is associated with the current branch along which the SPMW is present (Figure 1) [*Brambilla and Talley*, 2008]. Transformation of the $27.2\sigma_\theta$ SPMW up to the $27.5\sigma_\theta$ SPMW, measured as the diapycnal flux across the 27.15–$27.45\sigma_\theta$ isopycnals, occurs along the Rockall Trough branch of the NAC, Central Iceland Basin branch of the NAC and the Subarctic Front. The transformation from the $27.5\sigma_\theta$ SPMW up to the $27.7\sigma_\theta$ SPMW occurs along the East Reykjanes Ridge Current, the Irminger Current, and the East and West Greenland Currents. For each current, SPMW is found on the warm side of the current and not at its core.

[66] 2. The transport of water, including SPMW, along an isopycnal is characterized by subduction and obduction events along its path. Thus, it is not correct to imagine transformation of an entire SPMW directly into the next denser SPMW, which is the simplified hypothesis of *McCartney and Talley* [1982]. We have shown that the surface layer that includes the $27.3\sigma_\theta$ SPMW incorporates water upwelled from the interior. The 27.4 and $27.5\sigma_\theta$ layers that include SPWM are instead characterized by net downwelling into the ocean interior, occurring along both the northeastward flow from the Iceland Basin and Rockall Trough to the Iceland-Faroe Ridge, and along the East Reykjanes Ridge Current. In light of the results described in the companion paper [*Brambilla and Talley*, 2008], where SPMW is observed within the mixed layer and not subducted as a low potential vorticity water mass into the interior, and the agreement with the North Atlantic entrainment rates reported in previous studies [e.g., *Steele et al.*, 1962; *Dickson and Brown*, 1994; *Saunders*, 1996], we interpret the SPMW positive formation (subduction) as water mass loss by entrainment into the deep overflows of the Irminger Sea and the Iceland Basin.

[67] 3. Finally, although the diapycnal volume flux is a dominant source of SPMWs, the contribution of isopycnal flux cannot be neglected. We infer, from estimating the geostrophic transport across the A24 WOCE section in the eastern North Atlantic subpolar gyre, that the isopycnal contribution to the SPMW throughput might be 10%–40% of the diapycnal flux.

[68] **Acknowledgments.** This study was supported by the National Science Foundation Ocean Sciences Division, through grants OCE-9529584 (WOCE) and OCE-0424893 (CLIMODE), to Scripps Institution of Oceanography. E. Brambilla also received support from the SIO graduate department.

References

Brambilla, E., and L. D. Talley (2008), Subpolar mode water in the northeastern Atlantic: 1. Averaged properties and mean circulation, *J. Geophys. Res.*, *113*, C04025, doi:10.1029/2006JC004062.

Conkright, M. E., et al. (2002), *World Ocean Database 2001*, vol. 1, *Introduction, NOAA Atlas NESDIS*, vol. 42, 167 pp., NOAA, Silver Spring, Md.

Dickson, R. R., and J. Brown (1994), The production of North Atlantic Deep Water: Sources, rates, and pathways, *J. Geophys. Res.*, *99*, 12,319–12,341.

Ganachaud, A. (2003), Large-scale mass transports, water mass formation, and diffusivities estimated from World Ocean Circulation Experiment (WOCE) hydrographic data, *J. Geophys. Res.*, *108*(C7), 3213, doi:10.1029/2002JC001565.

Garrett, C., and A. Tandon (1997), The effects on water mass formation of surface mixed layer time-dependence and entrainment fluxes, *Deep Sea Res., Part I*, *44*, 1991–2006.

Garrett, C., K. Speer, and E. Tragou (1995), The relationship between water mass formation and surface buoyancy flux, with application to Phillips' Red Sea model, *J. Phys. Oceanogr.*, *25*, 1696–1705.

Grist, J. P., and S. A. Josey (2003), Inverse analysis adjustment of the SOC air-sea flux climatology using ocean heat transport constraints, *J. Clim.*, *16*, 3274–3295.

Gulev, S., B. Barnier, H. Knochel, J. M. Molines, and M. Cottet (2003), Water mass transformation in the North Atlantic and its impact on the meridional circulation: Insights from ocean model forced by NCEP-NCAR reanalysis surface fluxes, *J. Clim.*, *16*, 3085–3110.

Hanawa, K., and L. D. Talley (2001), Mode waters, in *Ocean Circulation and Climate—Observing and Modelling the Global Ocean*, edited by G. Siedler, J. Church, and J. Gould, pp. 372–386, Academic Press, San Diego, Calif.

Isemer, H.-J., and L. Hasse (1987), *The Bunker Climate Atlas of the North Atlantic Ocean*, vol. 2, *Air-Sea Interaction*, 218 pp., Springer, New York.

Krauss, W. (1986), The North Atlantic Current, *J. Geophys. Res.*, *91*, 5061–5074.

Large, W. K., and A. J. G. Prince (2001), Ocean surface water mass transformation, in *Ocean Circulation and Climate–Observing and Modelling the Global Ocean*, edited by G. Siedler, J. Church, and J. Gould, pp. 317–336, Academic Press, San Diego, Calif.

Lumpkin, R., and K. Speer (2003), Large-scale vertical and horizontal circulation in the North Atlantic Ocean, *J. Phys. Oceanogr.*, *33*, 1902–1920.

Marsh, R. (2000), Recent variability of the North Atlantic thermohaline circulation inferred from surface heat and freshwater fluxes, *J. Clim.*, *13*, 3239–3260.

Marshall, J., D. Jamous, and J. Nilsson (1999), Reconciling thermodynamic and dynamic methods of computation of water-mass transformation rates, *Deep-Sea Res., Part I*, *46*, 545–572.

Marshall, J. C., A. J. G. Nurser, and R. G. Williams (1993), Inferring the subduction rate and period over the North Atlantic, *J. Phys. Oceanogr.*, *23*, 1315–1329.

Masuzawa, J. (1969), Subtropical mode water, *Deep-Sea Res.*, *16*, 463–471.

McCartney, M. S. (1982), The subtropical recirculation of mode waters, *J. Mar. Res.*, *40*(suppl.), 427–464.

McCartney, M. S., and C. Mauritzen (2001), On the origin of the warm inflow to the Nordic Seas, *Prog. Oceanogr.*, *51*, 125–214.

McCartney, M. S., and L. D. Talley (1982), The Subpolar Mode Water of the North Atlantic, *J. Phys. Oceanogr.*, *12*, 1169–1188.

McCartney, M. S., and L. D. Talley (1984), Warm-to-cold water conversion in the northern North Atlantic, *J. Phys. Oceanogr.*, *14*, 922–935.

Nurser, A. J. G., R. Marsh, and R. Williams (1999), Diagnosing water mass formation from air-sea fluxes and surface mixing, *J. Phys. Oceanogr.*, *29*, 1468–1487.

Paillet, J., and M. Arhan (1996), Oceanic ventilation in the eastern North Atlantic, *J. Phys. Oceanogr.*, *26*, 2036–2052.

Perez-Brunius, P., T. Rossby, and D. R. Watts (2004), Transformation of the warm waters of the North Atlantic from a geostrophic streamfunction perspective, *J. Phys. Oceanogr.*, *34*, 2238–2256.

Pickart, R., F. Straneo, and G. W. K. Moore (2003), Is Labrador Sea Water formed in the Irminger Sea?, *Deep Sea Res., Part I*, *50*, 23–52.

Qiu, B., and R. X. Huang (1995), Ventilation of the North Atlantic and North Pacific: Subduction versus obduction, *J. Phys. Oceanogr.*, *8*, 2374–2390.

Read, J. F. (2001), CONVEX-91: Water masses and circulation of the northeast Atlantic subpolar gyre, *Prog. Oceanogr.*, *48*, 461–510.

Saunders, P. M. (1996), The flux of dense cold overflow water southeast of Iceland, *J. Phys. Oceanogr.*, *26*, 85–95.

Schmitz, W. J. (1995), On the interbasin-scale thermohaline circulation, *Rev. Geophys.*, *33*, 151–174.

Schmitz, W. J., and M. S. McCartney (1993), On the North Atlantic circulation, *Rev. Geophys.*, *31*, 29–49.

Speer, K. (1997), A note on average cross-isopycnal mixing in the North Atlantic Ocean, *Deep Sea Res., Part I*, *44*, 1981–1990.

Speer, K., and E. Tziperman (1992), Rates of water mass formation in the North Atlantic Ocean, *J. Phys. Oceanogr.*, *22*, 93–104.

Speer, K. G., H. J. Isemer, and A. Biastoch (1995), Water mass formation from revised COADS data, *J. Phys. Oceanogr.*, *25*, 2444–2457.

Steele, J. H., J. R. Barrett, and L. V. Worthington (1962), Deep currents south of Iceland, *Deep Sea Res.*, *9*, 465–474.

Talley, L. D. (1999), Mode waters in the subpolar North Atlantic in historical data and during the WOCE period, *WOCE Newsl.*, *37*, 3–6.

Talley, L. D. (2003), Shallow, intermediate, and deep overturning components of the global heat budget, *J. Phys. Oceanogr.*, *33*, 530–559.

Tandon, A., and L. Zhao (2004), Mixed layer transformation for the North Atlantic for 1990–2000, *J. Geophys. Res.*, *109*, C05018, doi:10.1029/2003JC002059.

Tziperman, E. (1986), On the role of interior mixing and air-sea fluxes in determining the stratification and circulation of the oceans, *J. Phys. Oceanogr.*, *16*, 680–693.

Valdivieso Da Costa, M., H. Mercier, and A. M. Treguier (2005), Effects of the mixed layer time variability on kinematic subduction rate diagnostics, *J. Phys. Oceanogr.*, *35*, 427–443.

Walin, G. (1982), On the relation between sea-surface heat flow and thermal circulation in the ocean, *Tellus*, *34*, 187–195.

E. Brambilla, P. E. Robbins, and L. D. Talley, Scripps Institution of Oceanography, University of California, San Diego, 9500 Gilman Drive, La Jolla, CA 92093-0230, USA. (elena.brambilla@gm.univ-montp2.fr)